Journal of the European Ceramic Society 20 (2000) 1023–1034

Evaluation of commercial nickel oxide powders for components in solid oxide fuel cells

Frank Tietz*, Francisco J. Dias, Dimitris Simwonis, Detlev Stöver

Research Centre Jülich, Institute for Materials and Processes in Energy Systems (IWV-1), D-52425 Jülich, Germany

Received 22 April 1999; received in revised form 9 September 1999; accepted 8 October 1999

Abstract

Various commercial nickel oxides were examined with respect to their relevant powder properties for application as anodes or anode substrates in solid oxide fuel cells (SOFC). The powders were characterized regarding their morphology, grain size distribution, BET surface and sintering behavior. Furthermore, anode substrates were produced from these powders together with yttria-stabilized zirconia (YSZ) powder. The sintering behavior, gas permeability and electrical conductivity of these components were determined and compared with the current standard material used for SOFC development at Research Centre Jülich. A comparison of the powder and component properties indicate a significant influence of the powder properties on the components produced.

Keywords: Anodes; Electrical properties; Fuel cells; NiO; Sintering; ZrO_2

1. Introduction

Fuel cells are electricity- and heat-generating components which directly convert the chemical energy of a fuel (hydrogen, natural gas, coal gas) and an oxidant (O_2, air) into electricity by means of an electrochemical process. Different types of fuel cells can be distinguished on the basis of the operating temperature and the nature of the electrolyte used (Table 1).

The flowing oxygen is catalytically reduced at the cathode and the O^{2-} ions formed are transported through the solid electrolyte due to the difference in oxygen potential between the anode and cathode compartment. On the anode side, the feed gas is oxidized by the hydrogen molecules reacting with the O^{2-} ions thus releasing electrons which flow back to the cathode via an external consumer. It is quite obvious that the electrocatalytic oxidation reaction of the hydrogen at the nickel can only proceed if the phase supplying O^{2-} is present and that electric current can only flow if the nickel forms continuous conduction paths in the porous combination of ceramic and metal (cermet) in order to transmit the electrons produced to the current collectors. The microstructure of the porous anode — and cathode — and the associated number of electrochemically active centers (three-phase boundaries) is thus of decisive significance for SOFC performance.

An SOFC uses an oxidic solid as the electrolyte material. This material must have sufficient ionic conductivity for O^{2-} ions, which is ensured by the high operating temperature. A thin self-supporting electrolyte film of stabilized or partially stabilized zirconia is most frequently used as the supporting component of the cells (Fig. 1, left). The so-called "substrate concept" of Research Centre Jülich represents a further development where the anode takes over the substrate function and a very thin electrolyte layer is deposited on this electrode (Fig. 1, right).[1–4]

Depending on the particular fuel cell type and the pre-conditioning of the feed gas, electrical conversion efficiencies of up to 70% should be achievable in future. Additional advantages in decentralized stationary energy production are often mentioned for the operation of fuel cells such as: low emissions of CO_2, CO, NO_x, SO_2, no dust, no noise disturbance, fuel and site flexibility, reduction of transmission losses and modularity.

The costs of fuel cells are still high at present and the technical level of development of the overall system is not yet mature for large-scale production. Since the ceramic membrane-electrodes assemblies have reached a much more advanced level of development and the anode substrate (Fig. 1, right) accounts for more than 90% of the ceramic material expenditure, however, it is

* Corresponding author. Tel.: +49-2461-615007; fax: +49-2461-2455.

E-mail address: f.tietz@fz-juelich.de (F. Tietz).

0955-2219/00/$ - see front matter
PII: S0955-2219(99)00271-X

Table 1
Materials for the membrane-electrode assembly of different fuel cells

	AFC[a]	PEMFC[b]	PAFC[c]	MCFC[d]	SOFC[e]
Operating temperature	343 K	373-393 K	473 K	923 K	1073–1273 K
Cathode	Pt	PtRu	Pt	(Ni,Li)O	$(La,Sr)MnO_3$
Electrolyte	Aqueous KOH	Organic polysulphonic acid (Nafion)	H_3PO_4	$(K,Li)CO_3$ in $LiAlO_2$ substrate	8YSZ
Anode	Pt	PtRu	Pt	NiCr	Ni/8YSZ

[a] AFC = alkaline fuel cell.
[b] PEMFC = proton exchange membrane fuel cell.
[c] PAFC = phosphoric acid fuel cell.
[d] MCFC = proton carbonate fuel cell.
[e] SOFC = solid oxide fuel cell.

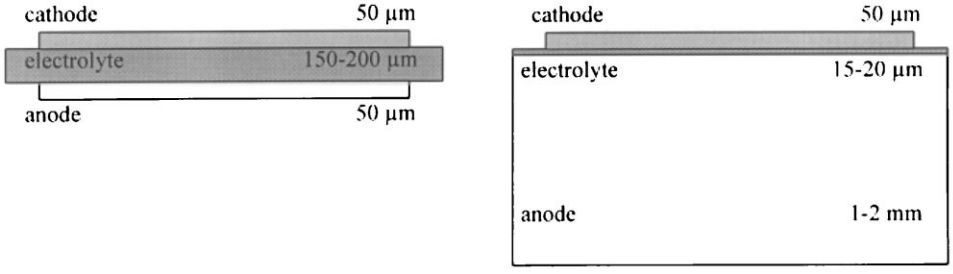

Fig. 1. Schematic SOFC set-up of a cell with a self-supporting electrolyte layer (left) as developed e.g. by Siemens[5] or Daimler-Benz/Dornier[6] and with an anode substrate as the supporting component (right) as produced at Research Centre Jülich[2].

meaningful to already start considering possibilities of saving material costs for this component at the present time. Low-cost nickel oxides are therefore being sought and attempts are also being made to replace the ceramic component (8 mol% Y_2O_3-stabilized ZrO_2, 8YSZ) in the substrate by cheaper oxides such as TiO_2 or Al_2O_3.[7]

Similar cost reductions programs have also been considered for tubular SOFCs, which are cathode supported cells.[8] In this attempt the high purity raw material La_2O_3 for the production of lanthanum manganite powder is replaced by lanthanide mixtures.

2. Component properties and choice of powder

A detailed overview of the whole spectrum of SOFC materials can be found in a paper by N. Q. Minh.[9] The materials currently used for fabricating SOFCs at Research Centre Jülich and their essential properties are summarized in Table 2.

Perovskite materials of the ABO_3 type are used as the cathode material. A frequently used material is lanthanum manganite ($LaMnO_3$) with substitutions of strontium or calcium at the A-site. Both A- and B-site substitutions have been performed on a large scale so that these oxidic alloys can be selected according to the demands made on their properties such as thermal expansion coefficient, electronic conductivity and stability under oxidizing atmosphere or chemical interaction with the electrolyte. In past years, a lot of SOFC developers produced the cathode powders themselves due to proprietary reasons or a lack of adequate commercial products. There are, however, today a limited number of chemical companies who supply even small quantities of any perovskite composition according to the customer's requirements.

8YSZ is commonly used for the fabrication of the electrolyte layer. At 1000°C this material displays sufficient electrical conductivity for O^{2-} ions of about 0.15 S/cm both in oxidizing and reducing atmospheres. For

Table 2
SOFC materials[2] and material characteristics

Component	Composition	Component thickness	Porosity	Conductivity (at 1273 K)
Cathode	$La_{0.65}Sr_{0.3}MnO_3$	50 µm	approx. 40%	$\geqslant$200 S/cm
Electrode	$Y_{0.15}Zr_{0.85}O_{1.93}$	15–20 µm	$\geqslant$96%	0.13–0.18 S/cm
Anode	50 wt.% Ni, 50 wt.% 8YSZ	1.5–2 mm	approx. 40%	300–400 S/cm
Interconnect	Fe 17Cr 1Al 1Si	approx. 3 mm	$\approx$100%	$\geqslant$1000 S/cm

application in the self-supporting electrolyte concept, layers with a thickness of 150 to about 200 μm are used to ensure sufficient inherent stability of the substrate. The transition to a substrate concept enables temperature reductions to be achieved because the loss of conductivity with decreasing temperature is compensated by the lower electrolyte thickness down to about 10 μm. While a few years ago there was a considerably greater number of suppliers for 8YSZ powders, the choice of powder has been perceptibly reduced because the size of the market has not fulfilled expectations and cost pressure has increased. An exhaustive examination of ten different commercial YSZ powders was undertaken by Ciacchi et al.[10] to identify an optimal powder for SOFC development in Australia. Such comparative studies were also performed by others.[11,12]

The most commonly applied anode material is a nickel/YSZ cermet; a mixture of nickel oxide and YSZ powder is used as the starting material. In the final structure of the electrode the nickel oxide is then reduced to nickel during the start-up phase of the cell or stack by the prevailing fuel atmosphere. The nickel serves as a catalyst for the oxidation reaction of the hydrogen and is finely dispersed around the YSZ particles. The function of the zirconia skeleton is to stabilize a porous electrode structure, to create an extended reaction zone by increasing the number of three-phase contact points and also to adapt the thermal expansion coefficient between the nickel and the other cell components. In the anode supported planar SOFC, an anode cermet with 40% porosity is used as the substrate, the microstructure displaying a pore structure which is graded towards the interface with the electrolyte.[2] Fig. 2 shows the microstructure of a membrane-electrodes assembly with a 15 μm thick electrolyte layer.

The demands made on the anode substrate such as good electrical conductivity, good gas permeability and fine-grained homogeneous microstructure can be realized by the powders currently used. At a stage of development where these demands on the component can be fulfilled reproducibly, consideration can be given as to whether it would not also be possible to satisfy the same demands with technical qualities costing approx. US$ 3–10/kg instead of using very good but expensive powder qualities.

In addition to the aspect of raw material prices, this addresses the general problem of whether a well-functioning component such as the membrane-electrodes assembly of the SOFC, currently based on high-quality powders, can also be realized by technical powder qualities. As an example, the substrate and in particular the nickel oxide was selected since the NiO used hitherto satisfies very high demands on quality (it is the only green NiO with an average grain size of <1 μm, cf. Table 3) and earlier studies with lower-grade NiO have shown that if the powder is appropriately conditioned

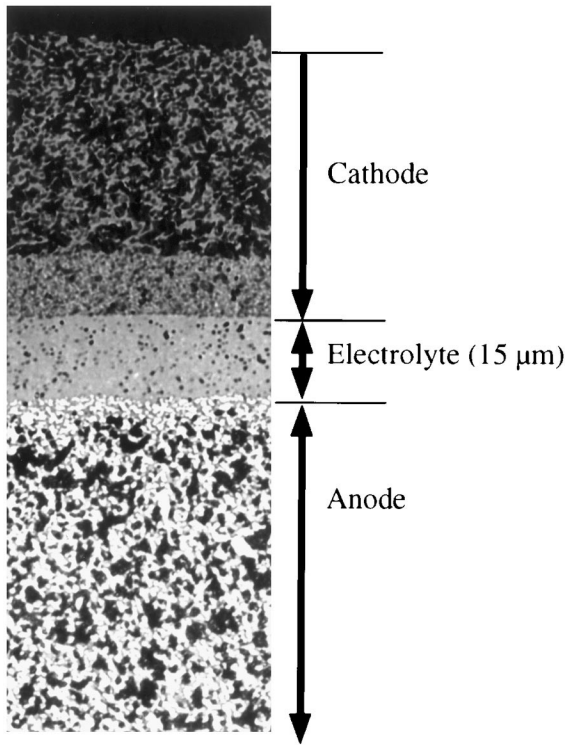

Fig. 2. Microstructure of a membrane-electrodes assembly.

effective anodes can also be produced by the screen-printing technique.[13]

3. Market research

A worldwide survey was conducted to obtain some idea of the NiO grades available on the market. Thirty companies were asked whether they could supply nickel oxides with the following properties:

- purity: $>99\%$,
- grain size distribution: $d_{50}<0.5$ μm or $d_{90}<3$ μm,
- BET surface: <10 m^2/g,
- price: < US$ 50/kg.

The powder properties were selected in such a way that fine powders which had, however, already been subjected to heat treatment — by analogy with the current standard powder — were to be filtered out in the inquiries. Many inquiries remained unanswered or were passed on to cooperating companies for a response. Of the ten answers received, there were just four companies who were of the opinion that they could fulfil the above-mentioned requirements and who were also prepared to supply samples for the fabrication of substrates. Apart from the standard powder (NiO-5), seven other NiO powders were therefore used for comparative studies (cf. Table 3).

Table 3
NiO powders investigated and their properties

Source	Name of variety	Abbr.	Color	Average grain size, d_{50} (μm), measured	Average grain size, d_{50} (μm), specified by manufacturer	BET surface (m^2/g), measured	BET surface (m^2/g), specified by manufacturer
Pharmacie de France	SPR	NiO-1	Olive green-grey	6.7	1.0-8.0	1.5	
harmacie de France	SPRM[a]	NiO-1A	Brown-grey	0.5	0.5-0.9	2.7	
Inco[b]	Grade F	NiO-2	Anthracite	0.6	approx. 1.0	55.7	
Inco[b]	Grade A	NiO-2A	Black	5.3	6.0-8.0	79.6	
Novamet[b]		NiO-3	Dark green	7.6	3.7	0.2	
J.T. Baker[c]		NiO-5	Grey-green	0.8	<3	4.3	
OMG[d]	No. 20	NiO-7	Black	14.7	14	47.0	40
Queensland[d]		NiO-8	Olive green	5.6		0.4	

Source	Abbr.	Particle morphology	Main impurity (ppm) measured	Main impurity (ppm) specified by manufacturer	Start of sintering (K)
Pharmacie de France	NiO-1	Rough hollow spheres of small primary particles	Co: 1448 Fe: 38	Fe: <100	1008
Pharmacie de France	NiO-1A	Very small, smooth and round	Co: 824 Fe: 71	Fe: <100	1013
Inco	NiO-2	Small smooth, in part agglomerated particles, high ultra-fine grain fraction	Na: 46 Fe: <5	Fe: <200	703
Inco	NiO-2A	Rough and microporous spheres or ellipsoids	Cu: 84 Fe: <5	Fe: <150	733
Novamet	NiO-3	Irregular, elongated agglomerates of smooth primary grains	Na: 62 Fe: 26	Fe: 25	1053
J.T. Baker	NiO-5	Small smooth, in part well-formed crystallites	Co: 95 Na: 88	Co: <2000 Na: <200	878
OMG	NiO-7	Rough, fissured microporous agglomerates	Na: 208	Na: 300	623
Queensland	NiO-8	Well-crystallized grains with smooth fracture surfaces	Mn: 425 Mg: 408	Mg: 600	1473

[a] No longer supplied.
[b] Supplied by Inco Specialty Powder Products.
[c] Standard powder.
[d] Supplied by German marketing partner D+H Dichem.

4. Experimental procedures

The powder morphology, grain size distribution, surface area (BET) and sintering behavior of the powders as delivered were characterized and the impurity of 27 elements determined in order to assess the influence of the powder properties on the component properties. Micrographs of the grain morphologies were collected using a scanning electron microscope (JSM T300, JEOL, Tokyo Japan). The grain sizes were measured by laser light scattering (laser-particle-sizer analysette 22, Fritsch, Idar-Oberstein, Germany) and the specific surfaces of the powders were determined using an adsorption apparatus (area-meter II, Ströhlein Instruments, Düsseldorf, Germany). For sintering experiments in a dilatometer (DIL 402C, Netzsch, Selb, Germany) pellets with 8 mm in diameter and 5 mm in thickness were fabricated from all the powders by uniaxial pressing with a pressure of 400 MPa. These pellets were heated in air at 3 K/min to a temperature of 1673 K and sintered at this temperature for 10 h.

For the fabrication of anode substrates the different NiO powders were treated as the standard NiO-5 powder, which was incorporated in these experiments as a reference. Because the fabrication process is already described elsewhere in more detail,[3,4,14] only a brief description is given here. The various powder mixtures of 8YSZ (Unitec, UK) and NiO, which had been ground together, were suspended in an ethanol binder resin solution and subsequently coated with the phenol aldehyde resin by adding water due to the insolubility of the binder.[4,14,15] Since the powders have different powder morphologies, some coating parameters such as binder fraction and the ratio of alcohol to water had to be adapted to the respective powder in order to achieve sufficient flowability and faultless sintering. The coated powder mixtures were then dried and filled into pressing dies. Pressing was performed at about 390 K and a pressing pressure of 0.4 MPa. The resin becomes viscous under these conditions and thus permits a very homogeneous density distribution in the green body.[3] The pressed substrates (either 50×50 mm or 100×100 mm

for fuel cell fabrication or 33 mm in diameter and 2 mm in thickness for basic studies) are then usually pre-sintered in a slow debinding and pre-sintering step at 1560 K in a chamber furnace. Since the sintering properties of the substrates were to be investigated, the binder was removed at 1073 K. The substrates were then first sintered in steps of 100 K up to 1673 K and then in 5 h intervals up to an overall duration of 20 h at maximum temperature. After each sintering step the specimen was cooled to room temperature and the shrinkage measured to determine the geometrical density. All substrates contained 55 wt% NiO and 45 wt% 8YSZ.

In addition to the series of experiments for the sintering studies, other substrates were presintered at 1560 K and finally sintered at 1673 K on a standard basis. These specimens were also used for gas permeability measurements[4] and after reduction of the NiO to metallic nickel at 1173 K in Ar/4% H_2 also for electrical conductivity measurements using a four-probe dc technique and silver paste for contacts. The measurements were carried out from 1173 K down to room temperature on specimens having the dimensions 20–25×5×2 mm. After reduction, all substrates contain 50 wt% Ni and 8YSZ.

For microstructural investigations the polished cross sections of the Ni/YSZ cermets were coated with an Fe_2O_3 interference layer to reduce the strong reflection of the Ni particles in the optical microscope. In this way it is easier to distinguish the three phases Ni, YSZ and pores.

5. Results and discussion

5.1. Powder properties of the nickel oxides

The color of the nickel oxides already indicated whether the powder was "calcined" NiO (dark grey to black) or "sintered nickel oxide" (green). Since the boundaries between these trade names are fluid and solely depend on the temperature of the thermal treatment, conclusions can be drawn from the color, i.e. the nonstoichiometry δ in the formula $Ni_{1-\delta}O$,[16] about the fabrication process. All the black nickel oxides indicated that sintering started at <773 K (Table 3), whereas with increasing green tones ranging from brown-gray through gray-green and green-gray to olive green an increasingly late start to sintering was observed.

As examples of the wide range of powder morphologies, Fig. 3 shows various scanning electron micrographs. The top two pictures show powders very probably prepared by spraying techniques. The standard powder (Fig. 3, center left)[2] consists of sub-μm primary particles present in the form of loose, irregular agglomerates. Powders NiO-1A and NiO-2 have a similar appearance, although the latter has a fairly high ultrafine-grain fraction reflected by the very high BET surface. Powder NiO-3 (Fig. 3, center right) is characterized by elongated and in part branched particles. Although the grains of NiO-7 are large and irregularly shaped, they have a fissured structure with a very high specific surface and, as can also be seen in Fig. 3 bottom left, may break fairly easily. The most obviously crystalline powder is NiO-8 (Fig. 3, bottom right), in which both well-formed crystal faces and smooth fracture surfaces can be seen.

Grain size measurement (cf. results in Table 3) showed that only two powders approximately fulfilled the requirement of a d_{50} value of <0.5 μm: NiO-1A and NiO-2. All other alternative powders had much larger grain sizes, especially NiO-7 with a d_{50} value of 14.7 μm.

All the black nickel oxides are characterized by a large surface area (Table 3), a further indication that thermal treatment during the production process was performed at not too high temperatures. This was revealed in particular when the sintering behavior of pressed test specimens was examined in a dilatometer (Fig. 4). From these sintering experiments the following results were obtained: (i) sintering of the black NiO powders (NiO-2, NiO-2A, NiO-7) began at $T<773$ K, (ii) the standard powder (NiO-5) displayed the highest sintering rates between 1073 and 1173 K and a slight increase in volume in the temperature range of $1473<T<1673$ K, (iii) the shrinkage behavior of powders NiO-1 and NiO-1A was similar to that of the standard powder but the maximum shrinkage rate (dL/dt) shifted to higher temperatures (Table 4), (iv) powders NiO-3 and especially NiO-8 had a low sintering activity which is reflected in the slight differences in density between the initial and final specimen densities (Table 4). The activation energies in Table 4 can be derived from the dilatometer curves using the equations

$$\left(\frac{(\Delta L/L_o)}{T}\right) = \text{const.} \times \exp\left(\frac{-nE_a}{RT}\right) \quad (1)$$

or

$$\left(\frac{\mathrm{d}(\Delta L/L_o)}{\mathrm{d}T}T\right) = \text{const.} \times \exp\left(\frac{-nE_a}{RT}\right) \quad (2)$$

where $\Delta L/L_o$ is the relative shrinkage at temperature T, E_a is the activation energy and n is a constant describing the sintering mechanism ($n=1$, 0.5 and 0.33 for viscous, volume or grain-boundary diffusion, respectively).[18] For the various nickel oxides the activation energies were determined by plotting $\ln [T\,d(\Delta L/Lo)/\mathrm{d}T]$ versus $1/T$ and setting $n=0.5$, because the sintering of NiO is governed by the self-diffusion of oxygen.[19,20] The resulting graphs with a linear region gave rather small activation energies (70–140 kJ/mol) for the nickel oxides NiO-2, NiO-2A, NiO-5 and NiO-7. For the other powders

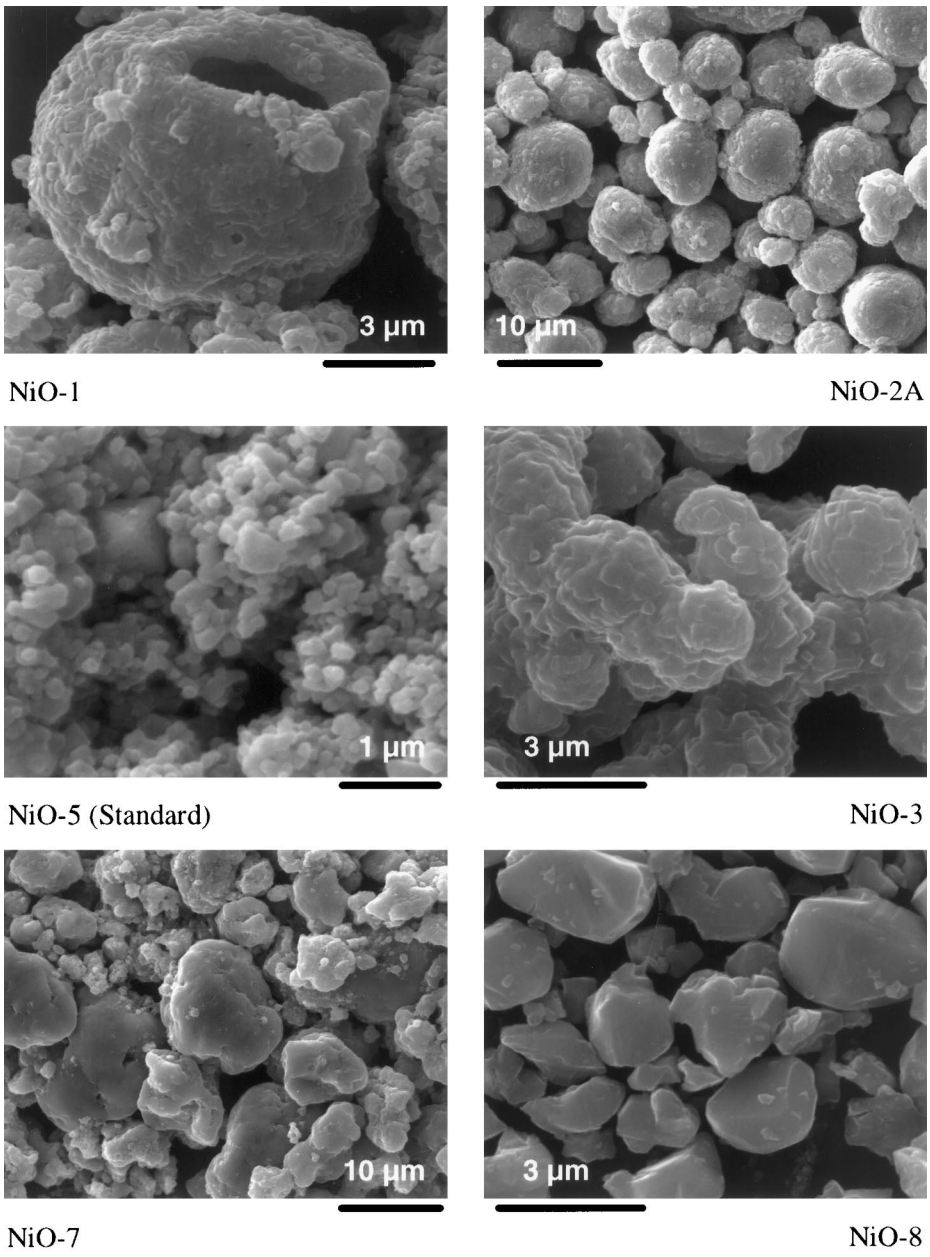

Fig. 3. Different particle morphologies of NiO powders.

(NiO-1, NiO-1A and NiO-3) higher values for E_a (170–330 kJ/mol) were obtained in accordance with previous sintering investigations.[19–21] Except of NiO-5, the two groups of NiO powders with different activation energies correspond to the classification of black- and green-colored powders. Because the crystal lattice of the green powders is well ordered, the larger activation energies are attributed to bulk diffusion. In previous investigations the sintering in NiO appeared to be controlled by oxygen lattice diffusion,[19,21] but it should be noted that the activation energies of oxygen and nickel self-diffusion as well as nickel diffusion along grain boundaries or dislocations fall in the regime of the measured E_a values.[21–24] Because of the similar activation energies, but also due to the different impurity levels (Table 3) and the observation that dopants can significantly change the sintering mechanism,[20] it cannot be excluded here, that the initial sintering mechanism is governed by only one diffusion process. In the case of the black powders it is reasonable to assume that the sintering mechanism is determined by a low-activated process, i.e. surface diffusion or short-range ordering of the crystal lattice.

The impurities were analyzed by mass spectrometry with inductively coupled plasma ionization (ICP-MS). Table 3 only shows the main impurity element and, where applicable, the type of atom specified by the manufacturers as the most frequent impurity. While iron was frequently specified as the main impurity, the

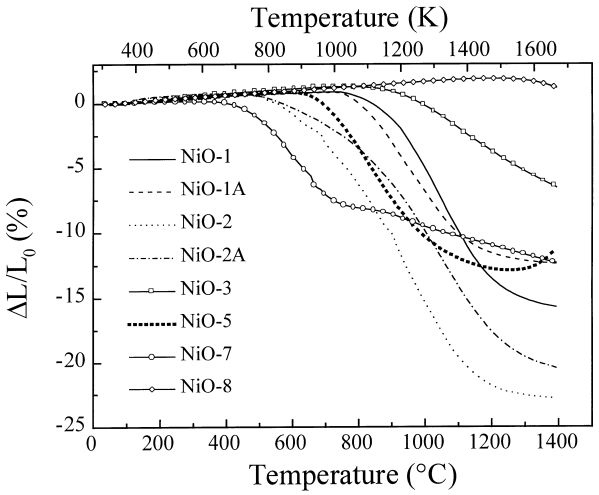

Fig. 4. Sintering behavior of NiO powders during heating up to 1673 K at 3 K/min.

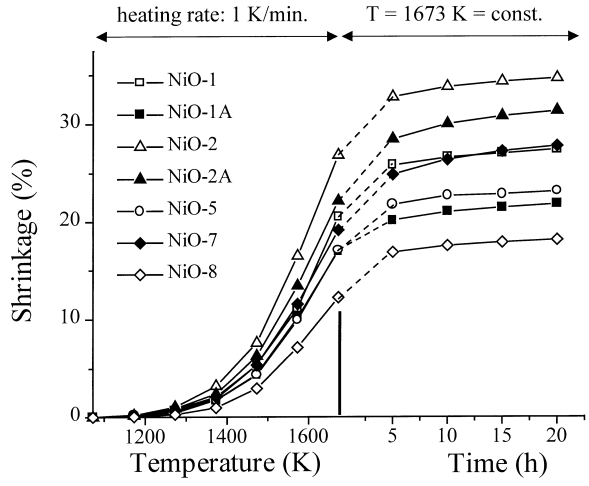

Fig. 5. Shrinkage characteristics of different NiO/YSZ substrates at sintering temperatures between 1073 and 1673 K (at 1 K/min) and subsequent dwell time of up to 20 h at 1673 K.

analytical results rather indicated a larger quantity of cobalt. In four of the eight powders good agreement with the manufacturer's analyses was observed.

5.2. Component properties

Together with the 8YSZ powder, anode substrates were fabricated from each NiO powder using standardized production parameters.[2–4,14] In spite of many attempts, the NiO-3 powder could not be coated with the phenol aldehyde resin and was, therefore, not considered for further investigations.

The shrinkage data of the NiO/8YSZ substrates are summarized in Fig. 5. Table 5 lists the shrinkages and relative densities after a sintering time of 10 h at 1673 K (cf. Table 4). As can be seen in Fig. 5, almost the same sintering shrinkages result for the standard substrate with NiO-5 and the substrate with NiO-1A in the dynamic, first part of the sintering experiments. Only sintering at constant sintering temperature leads to slightly different shrinkages for the two substrates.

The activation energies listed in Table 5 were determined from the shrinkage data during the heating period between 1173 and 1673 K (Fig. 5) with the aid of Eq. (1) and assuming grain boundary diffusion[12,18,25] ($n = 0.33$). It was assumed that the rapid heating and cooling cycles make a negligible contribution to the measurement of length in comparison to the length changes during slow heating. Activation energies in the range of 380–470 kJ/mol were determined for all the substrates except the specimen with NiO-8, which yielded a greater activation energies of 530 kJ/mol. Because in this case the NiO did not contribute significantly to the sintering process (cf. Fig. 4), the shrinkage and also the activation energy can be attributed to the sintering of the 8YSZ. Indeed, the value agrees well with activation energies reported previously.[12,18,26] Therefore, it can be assumed that the addition of sinterable NiO reduces the activation energy of sintering of NiO/8YSZ composites by about 100 kJ/mol.

No significant change in the sequence of green densities (d_a) can be identified in Tables 4 and 5 between the pure, pressed NiO specimens and the substrate specimens, i.e. the NiO powders have a perceptible influence on the properties of the anode substrates until after sintering. Furthermore, a comparison of the density differences achieved reveals that the sintering properties of the NiO powders also have a major influence on the sintering

Table 4
Sintering data for NiO powder compacts after 10 h at 1673 K in the dilatometer experiment

Powder	NiO-1	NiO-1A	NiO-2	NiO-2A	NiO-3	NiO-5	NiO-7	NiO-8
Relative initial density, d_a (%)[a]	47.2	59.7	43.1	39.8	59.9	55.9	51.4	64.6
Relative final density, d_e (%)[a]	78.9	93.6	90.9	80.4	82.5	83.7	83.3	70.4
Density difference, Δd (%)	31.7	33.9	47.8	40.6	22.6	27.8	31.9	5.8
Temperature (K) of maximum shrinkage rate	1313	1183	1193	1333	1358	1113	933	>1673
Activation energy, E_a (kJ mol^{-1})	206 ± 5	173 ± 8	70 ± 4	77 ± 1	323 ± 10	84 ± 5	137 ± 6	–
Considered temperature interval (K) for E_a	1028–1298	1038–1178	778–1298	768–1328	1088–1238	968–1118	628–848	–

[a] Related to the theoretical density $d_{th,\ NiO} = 6.81$ g/cm^3, calculated from the crystallographic lattice parameters.[17]

properties of the NiO/YSZ substrates. The greatest density difference thus arises for NiO-2, both for the pure powder and for the anode substrate, whereas the smallest density difference is found for NiO-8. The other powders are arranged between these two powders in a similar sequence in both series of experiments, with the processing steps (particularly grinding) and the YSZ powder added influencing the density data to different extents. Conditioning of the starting material as well as the NiO/YSZ ratio also significantly influence the sintering properties of anode materials.[13,27]

The results of gas permeability at room temperature and electrical conductivity measured at 1073 K are compiled in Table 6. The results of the sintering and gas permeability measurements show that the specimens with the highest sintering density (NiO-1A and NiO-2) also have the lowest gas permeability. In the reduced state, NiO-8 has approximately the same porosity as NiO-1A and NiO-2A but clearly lower gas permeability, which points to different pore structures or stronger densifications in the boundary regions of the compact. Although the functional properties, i.e. gas permeability and electrical conductivity, show an expected contrary course,[14] where the permeability decreases with rising density and the conductivity increases, no uniform trend is observed as a function of the measured densities or porosities. This indicates that, in addition to porosity, microstructural properties (grain sizes, pore structure, density gradients) are also of significance.

5.3. Microstructure-property-relationships and powder-component-relationships

In order to use the special microstructural features of the cermets for evaluating the workability of the powders and the physical properties achieved, ceramographic cross sections of the reduced test specimens were prepared. Fig. 6 shows the different microstructures of the fabricated cermets. The white areas are Ni particles, the YSZ particles appear gray and the pores black.

As already described elsewhere,[4,14] the standard material, YSZ and NiO-5, shows a very homogeneous distribution of all three phases. The microstructures of NiO-1 and NiO-1A cermets are comparable with the standard and display a very homogeneous Ni distribution with even finer Ni particles, which are effectively encapsulated by YSZ. The microstructure with NiO-1A is somewhat more densely sintered than that with NiO-1 or NiO-5 thus resulting in lower gas permeabilities in comparison to the standard material. The electrical conductivities of all three cermets are similar and vary between 600 and 900 S/cm (Table 6).

The microstructure with NiO-2 has slightly coarser Ni particles than in the cermet of NiO-1 and NiO-1A, some of which are up to 10 μm in size and already strongly interlinked. As can be seen from Table 6, the cermet with NiO-2 is most strongly compacted and its conductivity is therefore perceptibly higher than in the

Table 5
Sintering data of NiO/YSZ anode substrates after 10 h at 1673 K

NiO powder in composite	NiO-1	NiO-1A	NiO-2	NiO-2A	NiO-5	NiO-7	NiO-8
Relative initial density, d_a (%)[ab]	33.6	41.8	25.8	26.6	36.2	31.3	47.6
Relative final density, d_e (%)[b]	83.0	84.8	87.3	76.7	76.1	84.5	80.7
Density difference Δd (%)	49.4	43.0	61.5	50.1	39.9	53.2	33.1
Linear shrinkage, S (%)	26.6	21.0	33.8	30.0	23.7	26.4	17.6
Activation energy, E_a (kJ mol^{-1})[c]	472 ± 23	464 ± 19	447 ± 26	450 ± 26	387 ± 10	415 ± 12	527 ± 27

[a] After debinding at 1073 K.
[b] Related to the theoretical density $d_{th} = 6.37$ g/cm^3, calculated from the crystallographic lattice parameters for each component[17] and assuming the rule of mixtures for volume fractions in the composite.
[c] Temperature interval 1173–1673 K.

Table 6
Properties of anode substrates sintered and reduced in a standard mode before and after NiO reduction

NiO powder in composite	NiO-1	NiO-1A	NiO-2	NiO-2A	NiO-5	NiO-7	NiO-8
Relative density, d_{ox} (%)[a]	79.0	80.5	83.5	74.2	72.6	71.7	69.1
Relative density, d_{red} (%)[b]	62.9	64.1	78.1	67.4	58.3	56.5	68.1
Gas permeability, $D_{ox}/10^{-11}$ (cm^2)	2.33	1.68	0	2.55	5.38	5.41	0.52
Gas permeability, $D_{red}/10^{-11}$ (cm^2)	7.71	4.57	0.35	6.90	9.96	12.19	3.18
Conductivity, $\sigma_{1073\ K}$ (S cm^{-1})	894	702	3990	447	657	78	300

[a] See footnote b Table 5.
[b] Related to the theoretical density $d_{th} = 7.14$ g/cm^3, calculated from the crystallographic lattice parameters fro each component[17] and assuming the rule of mixtures for volume fractions in the cermet.

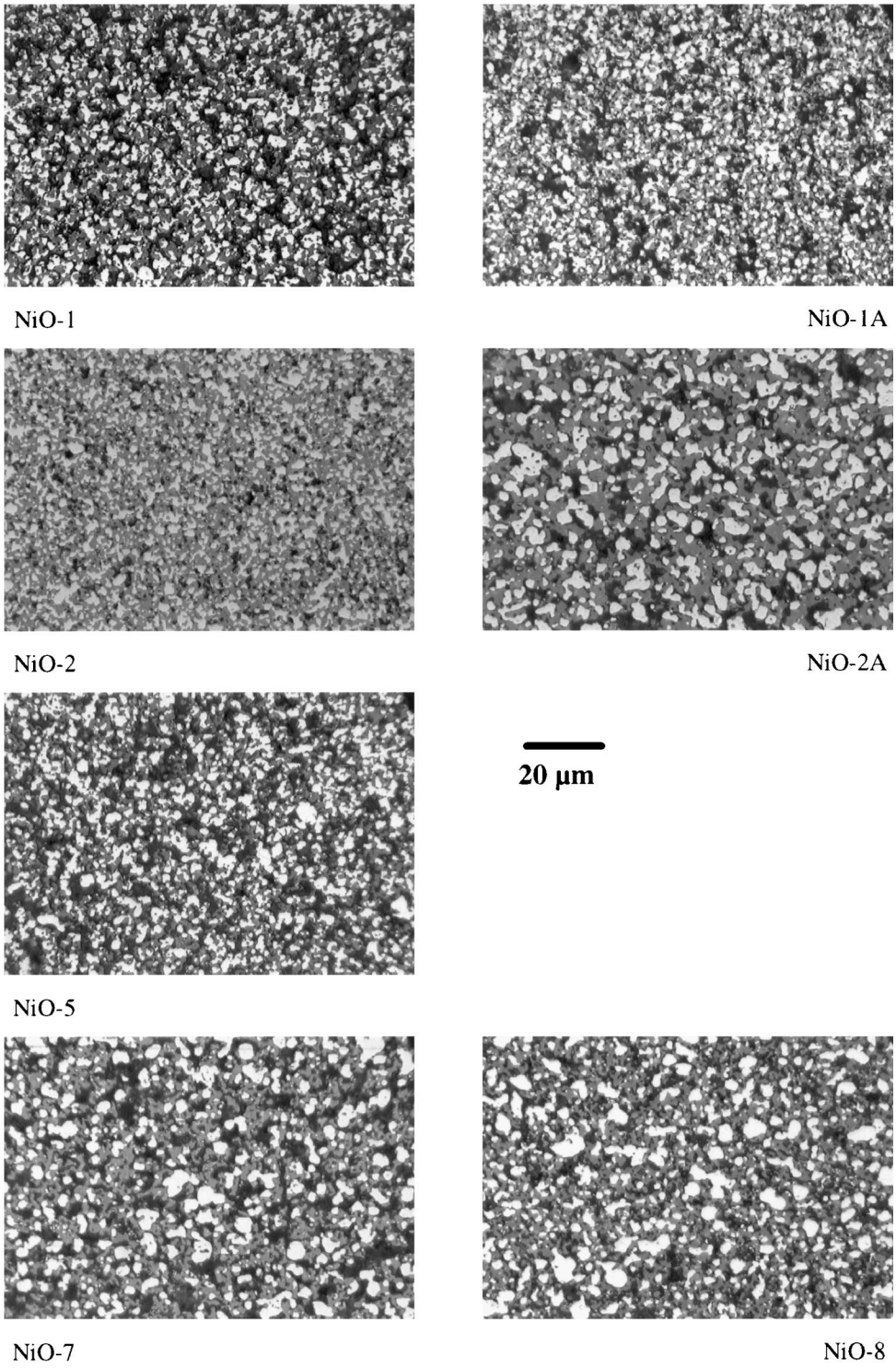

Fig. 6. Microstructure of Ni/YSZ cermets; white: Ni, gray: YSZ, black: pores.

other specimens. The cermet with NiO-2A also displays a distinctly coarser microstructure, both of Ni and of YSZ. While the grain size distribution of the Ni roughly corresponds to that of the NiO starting powder, and the grinding process before coating with resin thus does not influence the NiO powder, it cannot be ruled out that the copper impurities in this NiO powder cause liquid-phase sintering of the YSZ phase.[28] An indication of this is the lack of small pores within the YSZ particles (cf. the microstructures of cermets with NiO-7 and NiO-8, Fig. 6) and the generally relatively large pore diameters, which in spite of similar density (to that of cermets with

NiO-1A and NiO-8, cf. Table 6) ensure superior gas permeability. A similar relationship between liquid-phase sintering, pore size and gas permeability has also been found for cermets of Ni/TiO_2.[7] No other relationships between impurities and sintering properties of NiO/YSZ composites, e.g. the activation energies determined, could be identified.

The cermet of NiO-7 also contains coarse Ni particles in its microstructure, which are not always homogeneously distributed. Only small Ni particles are primarily dispersed in the YSZ matrix. Furthermore, in comparison to the other cermets, the porosity is high, which explains the very good gas permeability. Both the insufficient homogeneity of the nickel and the high porosity lead to an unsatisfactory interlinkage of the Ni particles thus resulting in low electrical conductivity. The constitution of the cermet made of NiO-8 powder is similar to that containing NiO-7, but with a better distribution of the Ni particles, whose size — as with NiO-7 — is up to about 10 μm. In these two cases as well, the grinding process only slightly influenced the NiO grain size. Due to the greater density and the smaller pore channels in the cermet with NiO-8, the functional properties change accordingly (Table 6).

In this study, the cermets with the NiO-1, NiO-1A and NiO-7 powders achieved similar properties to the standard cermet with NiO-5 powder, however, only for individual properties. Similarly good electrical conductivities were obtained with NiO-1 and NiO-1A powders, and correspondingly good gas permeability values with somewhat greater porosity with NiO-7 powder. A combination of the two opposite functional properties — using the standardized processing steps — was not achieved at the first attempt for any of the cermets studied. However, it seems possible to achieve similar properties and qualities of the component using the above mentioned nickel oxide powders by changing slightly the fabrication process of the anode substrates. The relatively poor conductivity of the NiO-7 cermet (Table 6) can be mainly attributed to the Ni particles which are still too coarse and the density which is too low. Both aspects lead to a reduction of electrical conductivity due to the smaller number of Ni-Ni contacts. In contrast, the standard NiO-5 cermet contains much finer and more homogeneously distributed Ni particles (Fig. 6). Since the NiO-7 powder is particularly characterized by the large average grain size of approx. 15 μm (Table 3), it is apparent that especially in this case fairly coarse Ni particles are found in the microstructure. The grinding and mixing process before fabricating the resin-coated powder was obviously not sufficient to destroy the large NiO agglomerates. In this case, the powder properties thus have a direct effect on the component properties. On the contrary, the coarse agglomerates of NiO-1 (Fig. 3) having a similar size as NiO-7 (Table 3) could be destroyed during the homogenization step resulting in a finely dispersed Ni phase in the cermet (Fig. 6). Therefore, the binding strength between the agglomerates is an important factor for the final microstructure of the cermets and a proper pretreatment has to be found for the NiO powder under consideration.

From the above results it was also possible to attribute easily the component properties of the YSZ and NiO-2 or NiO-8 anode substrates to the raw material properties. After thermal treatment, the high sintering activity of NiO-2 leads to a very high density, which for its part explains the high conductivity of the cermet and the low gas permeability. The characteristic feature of NiO-8 powder is the high green density of the compact and the low sintering activity. The resulting porosity is, therefore, in the range of the other nickel oxides. In contrast, the low gas permeability of this substrate can only be explained by a microstructural peculiarity of the component since the substrates with comparable density display significantly greater permeability values. The almost unchanged relative density before and after reduction is striking for this cermet, whereas the other cermets generally display a roughly 15% reduction in density (apart from the NiO-2 cermet with 5.5% and the NiO-2A cermet with 6.6%). All cermets deviating from this density change showed a perceptible deviation from the initial geometry after reduction and thus were not dimensionally stable. It is therefore not advisable to use these three NiO powders for future developments without changing the processing route.

With regard to the long-term stability of SOFC components, it is necessary that the anode substrates exhibit high (>100 S/cm) electrical conductivity during service life of 40,000 h or longer. The electrical properties can deteriorate during operation due to nickel diffusion leading to grain coarsening and loss of electrical contact between the grains.[9,29] A systematic investigation of the nickel agglomeration has been carried out recently[30] and revealed that the microstructure, especially the homogeneity as well as the Ni and pore size, has a significant influence on the contiguity of the nickel phase and the loss of electrical conductivity. Therefore, it can be expected that the cermets with NiO-1, NiO-1A, NiO-2, and NiO-5 will have a better long-term performance than the coarser cermets shown in Fig. 6.

6. Conclusions

It is possible to approximate the properties of the NiO/YSZ substrates of NiO-1, NiO-1A, NiO-2A and NiO-7 powders to the standard values by varying the processing steps, particularly for the grinding, pressing and sintering conditions. Powders with higher sintering activity than the standard material permit a cell fabrication in which the substrate-electrolyte system can be

jointly sintered at much lower temperatures and still achieves sufficient shrinkage to support densification of the electrolyte. NiO powders with lower sintering activity than the standard material can, on the other hand, be added to the present starting powder in order to optimize the joint shrinkage of substrate and electrolyte. From these examples, it may be seen that each of the NiO powders investigated can contribute towards achieving a certain development goal and can be utilized as an additional parameter for optimizing components or component combinations.

In conclusion, it can be established that in only a few cases do the powder properties investigated also determine the component properties, namely, whenever the mixing and grinding process only influences the powder characteristics to a slight degree. All powder mixtures which were further processed "undamaged" after this mechanical stressing also displayed typical properties of the raw material in the further course of the investigations or enabled conclusions to be drawn about them:

- NiO-2: The most finely grained powder with the highest sintering activity; it was not possible to reduce the high fraction of fine primary particles by any of the process steps. High sintering activity and shrinkage was retained.
- NiO-5: Also a fine powder which therefore displays good electrical conductivity with high porosity.
- NiO-7: Large powder particles which were not sufficiently ground thus resulting in a poor conductivity of the cermet.
- NiO-8: Very good crystallinity and hardness of the powder particles, grinding thus did not have any positive influence on the poor sintering activity.

In individual cases, it was, thus, also possible to identify relations between the raw material and component. In general, component properties can only be predicted from or correlated with powder properties if the powders for component fabrication remain largely unchanged. However, usually typical powder properties are changed during the processing steps (e.g. grinding, sieving, etching, reacting with additives etc.) in such a way that it becomes impossible to predict component properties.

Acknowledgements

The authors wish to thank the following colleagues for their experimental contributions to this paper: Mr G. Blaß (BET surface measurement), Dr W. Fischer (SEM study), Mr H. Hoven and Mrs R. Fisseler (ceramography), Dr U. Seeling and Mrs E. Lawin (chemical analyses), and Mr H. Wesemeyer (grain size determination). Furthermore, thanks are due to all contact persons at the suppliers for their kind support.

References

1. de Haart, L. G. J., Hauber, Th., Mayer, K. and Stimming, U. Electrochemical performance of an anode supported planar SOFC system. In *Proceedings of the 2nd European SOFC Forum*, (Oslo, Norway, May 1996). Vol. 1, Ed. B. Thorstensen, European Solid Oxide Fuel Cell Forum, Dr. U. Bossel, Oberrohrdorf, Switzerland, 1996, pp. 229–236.
2. Buchkremer, H. P. Diekmann, U., de Haart, L. G. J., Kabs, H., Stimming, U., Stöver, D. Advances in the anode supported planar SOFC technology. pp. 160–170 In *Proceedings of the 5th International Symposium on Solid Oxide Fuel Cells (SOFC-V)*, (Aachen, Germany, June 1997). Ed. U. Stimming, S. C. Singhal, H. Tagawa, W. Lehnert, The Electrochem. Soc., Pennington, NJ, 1997, pp. 160–170.
3. Buchkremer, H. P., Diekmann, U., Stöver, D. Components manufacturing and stack integration of an anode supported planar SOFC system, In *Proceedings of the 2nd European SOFC Forum*, Oslo, Norway, Vol. 1, May 1996, Ed. B. Thorslensen, pp. 221–228.
4. Simwonis, D., Naoumidis, A., Dias, F. J., Linke, J. and Moropoulou, A., Material characterization in support of the development of an anode substrate for solid oxide fuel cells. *J. Mater. Res.*, 1997, **12**, 1508–1518.
5. Blum, L., Drenckhahn, W., Greiner, H., Ivers-Tiffée, E. Multi-kW-SOFC development at Siemens. In *Proceedings of the 4th International Symposium on Solid Oxide Fuel Cells (SOFC-IV)*, Yokohama, Japan, June 1995, Ed. M. Dokiya, O. Yamamoto, H. Tagawa, S. C. Singhal, The Electrochem. Soc., Pennington, NJ, 1995, pp. 163–172.
6. Stolten, D., Späh, R., Schamm, R. Status of SOFC development at Daimler-Benz/Dornier. In *Proceedings of the 5th International Symposium on Solid Oxide Fuel Cells (SOFC-V)*, Aachen, Germany, Ed. U. Stimming, S. C. Singhal, H. Tagawa, W. Lehnert, The Electrochem. Soc., Pennington, NJ. 1997, pp. 88–93.
7. Tietz, F., Dias, F. J., Naoumidis, A. Novel anode substrates for planar solid oxide fuel cells. In *Proceedings of the 3rd European SOFC Forum*, Nantes, France, June 1998, Vol. 1, Ed. Ph. Stevens, European Solid Oxide Fuel Cell Forum, Dr. U. Bossel, Oberrohrdorf, Switzerland, 1998, pp. 171–180.
8. Singhal, S. C. Recent progress in tubular solid oxide fuel cell technology, In *Proceedings of the 5th International Symposium on Solid Oxide Fuel Cells (SOFC-V)*, (Aachen, Germany, June 1997). Ed. U. Stimming, S. C. Singhal, H. Tagawa, W. Lehnert, The Electrochem. Soc., Pennington, NJ, 1997, pp. 37–50.
9. Minh, N. Q., Ceramic fuel cells. *J. Am. Ceram. Soc.*, 1993, **76**, 563–588.
10. Ciacchi, F. T., Crane, K. M. and Badwal, S. P. S., Evaluation of commercial zirconia powders for solid oxide fuel cells. *Solid State Ionics*, 1994, **73**, 49–61.
11. Männer, R., Ivers-Tiffée, E., Wersing, W. Characterization of YSZ electrolyte materials with various yttria contents. In *Proceedings of the 2nd International Symposium on Solid Oxide Fuel Cells (SOFC-II)*, Athens, Greece, July 1991. Ed. F. Grosz, P. Zegers, S. C. Singhal, O. Yamamoto, Commission of the European Community, Brussels, Belgium, 1991, pp. 715–725.
12. Gibson, I. R., Dransfield, D. P. and Irvine, J. T. S., Sinterability of commercial 8 mol% yttria-stabilized zirconia powders and the effect of sintered density on the ionic conductivity. *J. Mater. Sci.*, 1998, **33**, 4297–4305.

13. Gupta, A. and Tietz, F. unpublished.
14. Simwonis, D., Dias, F. J., Naoumidis, A., Stöver, D. Manufacturing of porous cermet substrates for solid oxide fuel cells by coat-mix process. In *Proceedings of the 5th European Conference on Advanced Materials, Processes and Applications (EUROMAT 97)*, Maastricht, Netherlands, Vol. 2, April 1997. Ed. L. A. J. L. Sarton, H. B. Zeedijk, Netherlands Society for Materials Science, Zwijndrecht, Netherlands, 1997, pp. 375–378.
15. Luhleich, H., Dias, F. J., Pflaum, P. and Nickel, H. The coat-mix process (Das Coat-Mix-Verfahren), KFA-report Jül-1221, Forschungszentrum Jülich, 1975.
16. *Gmelins Handbook of Inorganic Chemistry*, 8th ed., 1966, Verlag Chemie, Weinheim, Volume Ni, Part B, (2), 376–396.
17. JCPDS-Database of the International Center for Diffraction Data (ICDD), Newton Square, PA, USA. Program package PCPDFWIN Version 1.30, data sheets 44-1159 (NiO), 04-0850 (Ni), and 30-1468 (8YSZ), 1997.
18. Young, W. S. and Cutler, I. B., Initial sintering with constant rates of heating. *J. Am. Ceram. Soc.*, 1970, **53**, 659–663.
19. Jiménez-Melendo, M., Domínguez-Rodríguez, A., Márquez, R. and Castaing, J., Sintering and Characterization Studies of NiO. *J. Physique (Coll.)*, 1986, **47 C1**, 385–390.
20. Senos, A. M. R., Santos, M. R., Moreira, A. P., Vieira, J.M. Grain boundary phenomena in the early stages of sintering of MO oxides. In *NATO ASI Series E, Vol. 173 - Surfaces and Interfaces of Ceramic Materials*. Ed. L.-C. Dufour, C. Monty, G. Petot-Ervas, Kluwer Academic Press, Dordrecht, Netherlands, 1989, pp. 553–563.
21. Anderson, H. U., Initial sintering of nickel(II)oxide. *Phys. Sintering*, 1973, **5**, 149–162.
22. Atkinson, A. and Taylor, R. I., The diffusion of Ni in the bulk and along dislocations in NiO single crystals. *Phil. Mag. A*, 1979, **39**, 581–595.
23. Atkinson, A. and Taylor, R. I., The diffusion of ^{63}Ni along grain boundaries in nickel oxide. *Phil. Mag. A*, 1981, **43**, 979–998.
24. Peterson, N. L. and Wiley, C. L., Point Defects and Diffusion in NiO. *J. Phys. Chem. Solids*, 1985, **46**, 43–52.
25. Theunissen, G. S. A. M., Winnubst, A. J. A. and Burggraaf, A. J., Sintering Kinetics and Microstructure Development of Nanoscale Y-TZP Ceramics. *J. Eur. Ceram. Soc.*, 1993, **11**, 315–324.
26. Upadhyaya, D. D., Kutty, T. R. G. and Ganguly, C. Densification behaviour and microstructural features of 3Y-TZP with and without additives. In *Proceedings of Science and Technology of Zirconia V*, Melbourne, Australia, August 1992. Ed. S. P. S Badwal, M. J. Bannister, R. H. J. Hannink, Technomic Publishing Co., Lancaster, PA, USA, 1993, pp. 310–320.
27. Matsushima, T., Ohrui, H. and Hirai, T., Effects of sinterability of YSZ powder and NiO content on characteristics of Ni-YSZ cermets. *Solid State Ionics*, 1998, **111**, 315–321.
28. Lemaire, L., Scholz, S. M., Valmalette, J. C., Lemaître, J. and Hofmann, H., Lowering of sintering temperature of 3Y-TZP by CuO additive. In *Proceedings of the 5th European Conference on Advanced Materials, Processes and Applications (EUROMAT 97)*. Maastricht, Netherlands, April 1997, vol. 2, Ed. L. A. J. L. Sarton, H. B. Zeedijt, Netherlands Society for Materials Science, Zwijndrecht, Netherlands, 1997, pp. 303–306.
29. Tietz, F., Simwonis, D., Batfalsky, W., Diekmann, U. and Stöver, D. Degradation phenomena during operation of solid oxide fuel cells. In *Proceedings 12th IEA Workshop on SOFC: Materials and Mechanisms in the frame of the IEA-Programme on Advanced Fuel Cells, Annex VII: SOFC under Real Operating Conditions*, Wadahl, Norway, January 1999. Ed. K. Nisancioglu, University of Trondheim, Norway, printed by and available from H. Nabielek, Forschungszentrum Jülich, Germany, pp. 1–13.
30. Simwonis, D. Optimierung der Anoden der Hochtemperatur-Brennstoffzelle durch Korrelation von Herstellungsverfahren, Gefüge und Eigenschaften; Jül-report 3678. Edited by Forschungszentrum Jülich, Germany, 1999